

## Supplementary information for

# Millimeter-wave to near-terahertz sensors based on reversible insulator-to-metal transition in vanadium dioxide

Fatemeh Qaderi et al.

### Supplementary Note 1: Antennas considerations

The same coupled antennas are simulated using finite element method (FEM). The variation of S parameters with respect to the conductivity of Vanadium dioxide ( $\text{VO}_2$ ) patch in the middle of one antenna follows the pattern shown in figs. 1(a) and 1(b)

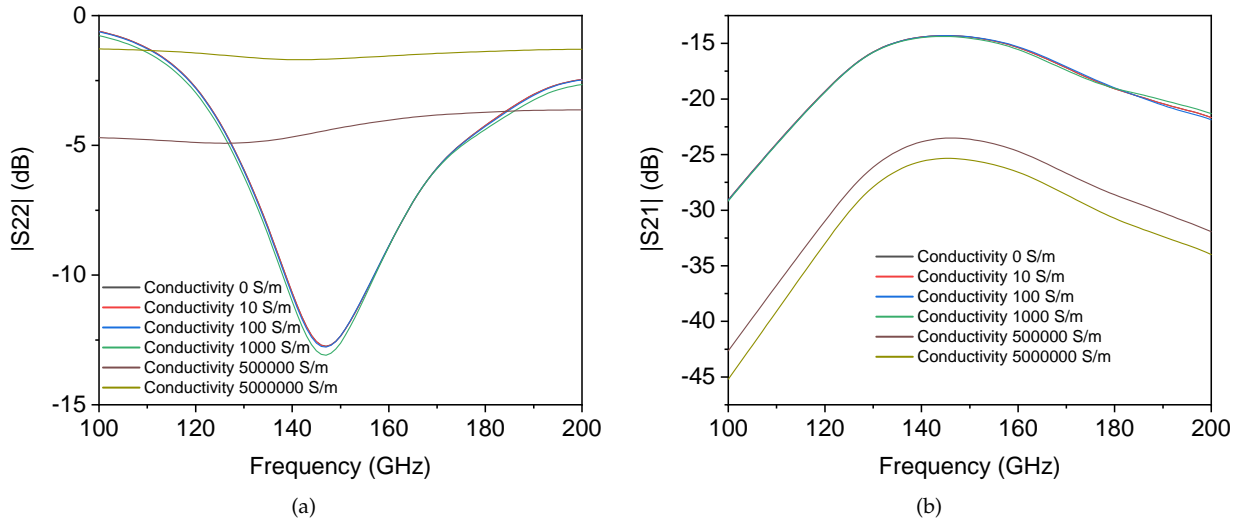


**Figure 1.** finite element method (FEM) simulations for the S parameters of the coupled antennas with respect to  $\text{VO}_2$  conductivity

In the antennas configuration of fig. 1 of the paper, only the receiver antenna is  $\text{VO}_2$ -loaded and DC-biased. The emitter antenna is only identical in the metallic pattern and no bias is applied to it. Port 1 is connected to the emitter, and its own return loss is revealed in fig. 2 (c) of the paper. The notch at 145 GHz shows the impedance match of this individual antenna to the ambient space around it. We should also notice that the return loss of the receiver antenna at port 2 is not the same as the one of port 1 due to the effect of  $\text{VO}_2$  leakage on the antenna's electromagnetic configuration. This is shown in fig. 2(a) where the peaks from  $|S_{21}|$  and  $|S_{11}|$  do not happen at the same frequencies.

$|S_{21}|$  represents the matching between the two antennas for a small portion of the power delivered by the emitter antenna to the outer space, i.e. about -10 dB at its maximum according to fig. 2 (d). The rest of the power is either absorbed by the ambience, or reflected back to the emitter antenna. In an optimized design, the resonance frequency for the return loss would be tuned exactly on the one of the insertion loss. In fig. 2 (d) we have at least 3 ranges where  $|S_{21}|$  reaches its highest values: 90 GHz, the range 120-150 GHz, and the range 200-220 GHz. These mutual partial-resonances between the two antennas are not necessarily at the same frequency of the individual antenna resonances, as a big portion of the power is already absorbed by the ambience. The amount of absorption is calculated by  $1 - |S_{11}|^2 - |S_{21}|^2$  and illustrated in fig. 2(b). The absorption is considerably high compared to the portion received by the other antenna, and this explains why the  $|S_{21}|$  and  $|S_{11}|$  curves are not perfectly complementary. On the other hand, the  $|S_{21}|$  is more complementary to the  $|S_{22}|$ .

In the biased antennas, we measured S parameters at different bias voltages. When applying the smallest power (-30 dBm), even the combination with a bias voltage up to 1.705 V does not lead to a phase transition (figs.

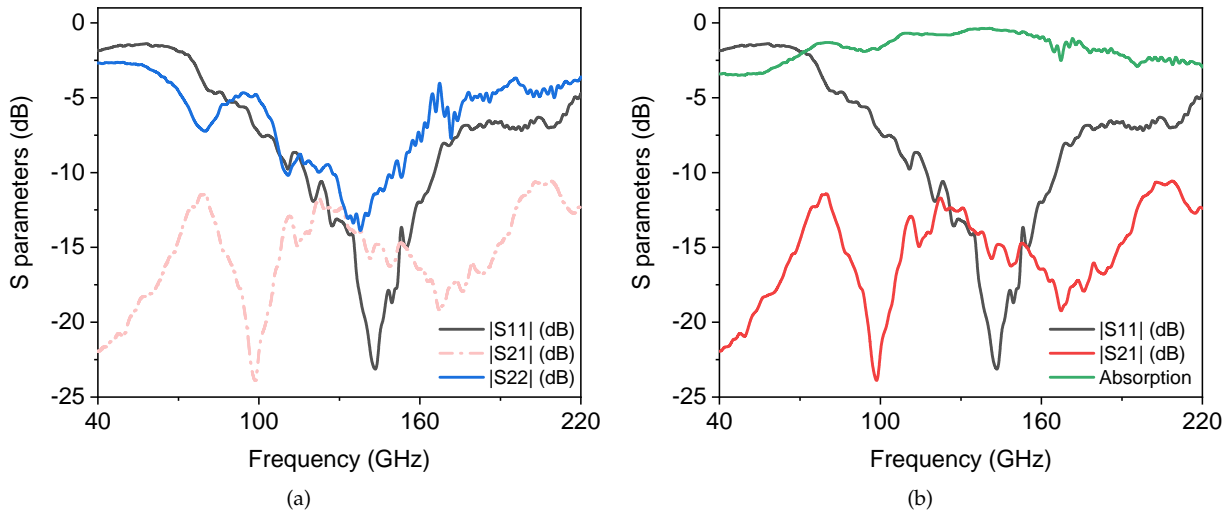


**Figure 2.** Measured S parameters for the antennas: (a) all the S parameters together. The peaks of  $|S_{11}|$  and  $|S_{22}|$  are not at the same frequencies. (b) the absorption of the emitted signal by the ambiance calculated by  $1 - |S_{11}|^2 - |S_{21}|^2$

3(a) and 3(b)), This is also the case with -20 dBm, while at the same voltage, the power levels higher than -10 dBm can trigger the phase transition. On the other hand, the power levels higher than -10 dBm are capable of triggering the phase transition even at lower bias voltages, such as 1.690 V (figs. 3(c) and 3(d)). A summary of all these figures combined is found in fig. 2 (d) of the paper.

#### Supplementary Note 2: VO<sub>2</sub> film investigation

The X-ray diffraction (XRD) of the VO<sub>2</sub> thin film which is deposited on a Si wafer with a 2  $\mu$ m SiO<sub>2</sub> buffer layer is shown in fig. ???. The main peak for the (011) phase is well pronounced in this measurement, which is required for the switching behavior. The measurement is repeated with a higher resolution in a smaller range to reduce the noise floor, as shown in the inset of fig. ??.

#### Supplementary Note 3: fabrication process

A layer of 2  $\mu$ m thermal oxide was grown on the surface of a high resistivity float zone (HRFZ) Silicon wafer. Then using pulsed laser deposition (PLD), we synthesized a 100-nm-thick VO<sub>2</sub> film on top of SiO<sub>2</sub>. The VO<sub>2</sub> film was patterned using photolithography on a 1.4  $\mu$ m layer of negative tone AZ nLof 2020 resist, developed in AZ 726 MIF developer. Wet etching of VO<sub>2</sub> was done in diluted 1:6 Cr etch solution. We stripped the resist by Oxygen plasma and putting it in remover 1165 for 30 minutes. For the second layer, 15 nm Cr was sputtered on the patterned substrate as an interface layer and the process was followed by the sputtering of 150 nm Au. The photolithography of the second layer was done with the same resist coating parameters and stripping method. The connections and the 2-terminal devices were completed by dry etching of the sputtered metal using a broad beam of Argon ions in an ion-beam-etcher. Resist stripping was done using the same method as the first lithography. The process flow is illustrated in fig. ??.

#### Supplementary Note 4: Operational range of the spike generator

We sweep the gate voltage in order to realize the operational region of the spike generator. It is worth noting that the circuit shows a hysteretic function of the gate voltage, in terms of the initial and final points of the gate voltage which supports oscillating conditions.

#### Supplementary Note 5: Setup considerations

While applying the RF signal to the antennas, the output power of the vector network analyzer (VNA) port

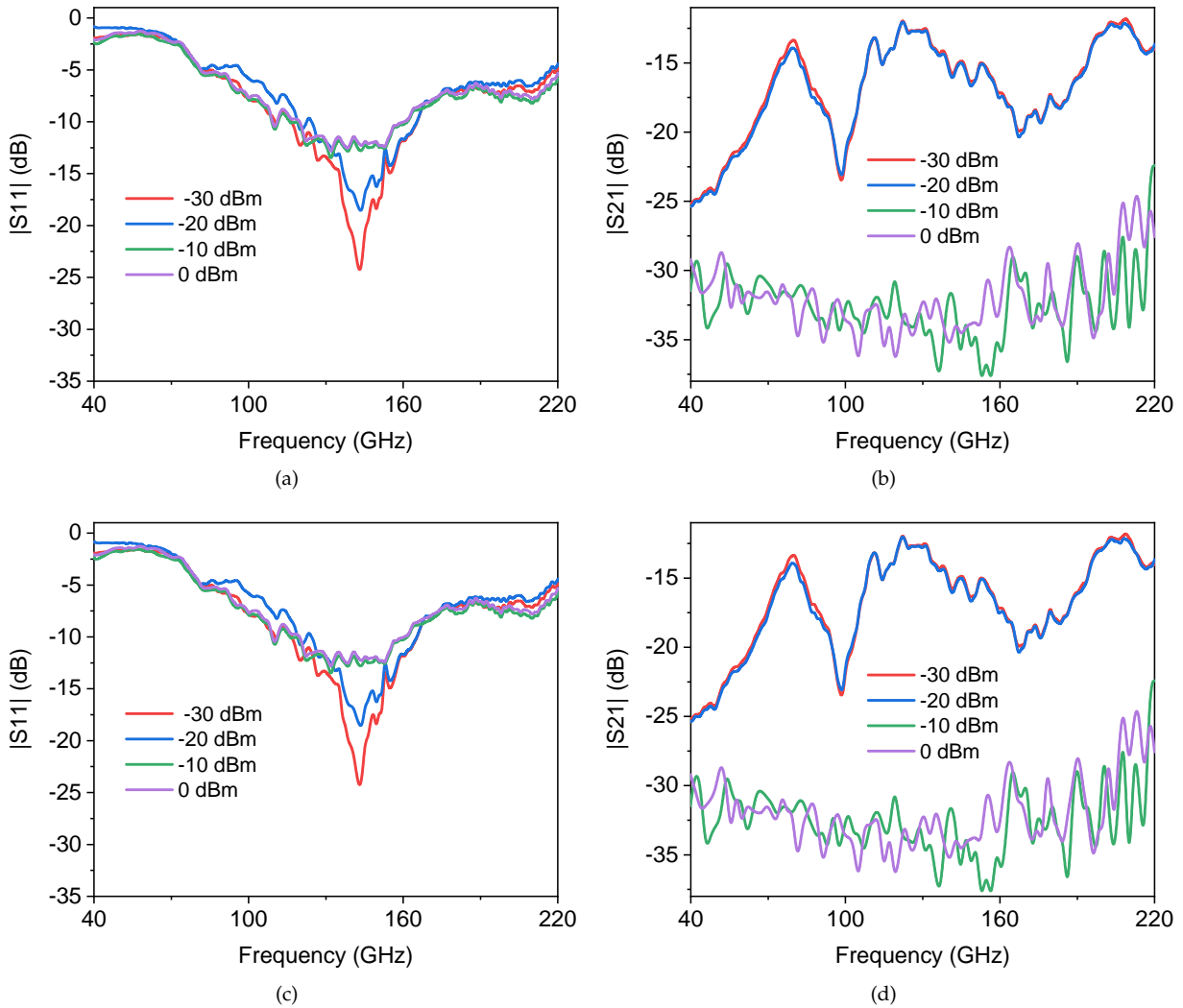


**Figure 3.** Measured S parameters for the biased antennas: (a)  $|S_{11}|$  for the bias voltage of 1.705 V. (b)  $|S_{21}|$  for the bias voltage of 1.705 V. (c)  $|S_{11}|$  for the bias voltage of 1.690 V. (d)  $|S_{21}|$  for the bias voltage of 1.690 V.

connected to the VO<sub>2</sub> patch was set to the lowest level at -50 dBm, and only the power level from the other port was looked upon. Therefore, the receiving port could be assumed as passive, with no intervening or direct injecting of power to the sensitive VO<sub>2</sub> part. Same measures were applied when connecting the ports to the CPW. More information about the VNA setup can be found here:

#### 220 GHz setup datasheet

Note. Every set of measurements applying RF signal are made with no displacement of the probes, whereas for higher temperatures the displacement was inevitable, which leads to very slight differences in S parameters under same other circumstances.

The dynamics of the sensor depend on the readout method. We have proposed two methods here, direct measurement of the threshold voltage based on VO<sub>2</sub> DC I-V characteristics, or the frequency measurement of the oscillator (AC method). Response time based on DC method: each measurement in this method is to locate the insulator-metal transition (IMT) threshold voltage. Hence, it depends on the speed of sweeping the DC voltage across the expected range of IMT voltages. For the proposed device of this paper, we have the range between 1.5 V to 1.7 V. The voltage resolution will determine the integration time. For a synthesized triangular signal, our oscilloscope operates at 2 GigaSamples/sec ([InfiniiVision 1000 X-Series Oscilloscopes](#)). We can set the slope for the voltage to progress at 1 mV/ns so that we have a resolution of <1 mV at this sampling rate. Therefore, a sweep of 200 mV takes 200 ns. The setup will be the combination of a normal resistor in series with the VO<sub>2</sub> impedance

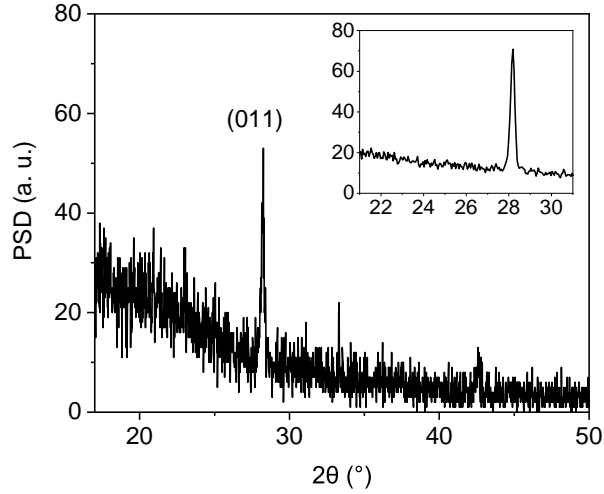


**Figure 4.** XRD of the 100-nm-layer of VO<sub>2</sub> thin film on top of Si/SiO<sub>2</sub> substrate, inset: the main peak with higher resolution

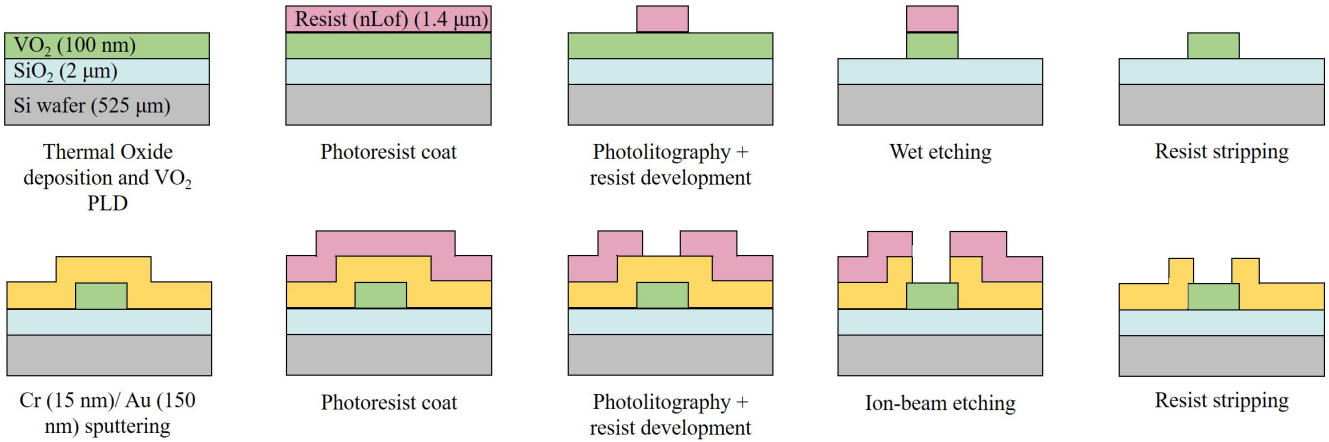


**Figure 5.** Summarized process flow of the 2-terminal devices along with the patterning for the antennas or coplanar waveguide (CPW)s

and the sampling would be from the shared node between the two. Each acquisition (of a measurement cycle) will take 200 ns, while this data needs to be analyzed offline, to extract the IMT threshold voltage for each cycle. One also needs to wait for the reset time in case of multiple acquisitions, which is at least a microsecond<sup>1</sup>. Response time based on AC method: in the VO<sub>2</sub>-based astable circuit we can scale the frequency of oscillations as high as the circuit operating point stays within a margin to maintain astability. This margin is achievable through the measurements discussed in the supplementary note 4: “operational range of the spike generator”. We used typical values for the circuit components: 150 nF capacitor along with the VO<sub>2</sub> impedances of 1.4 kΩ and 60 Ω for “off” and “on” states, respectively. That leads to a free-running oscillation frequency around 3250 Hz.

The period of each cycle provides a sampled data point. Being exposed to the radiation, the periods go shorter, so the maximum waiting time to collect a single data point would be  $\frac{1}{3250\text{Hz}} = 308\mu\text{s}$ .

For the spectral bandwidth, we consider the VO<sub>2</sub> switching response time, which is order of a nanosecond for IMT and order of a microsecond for MIT<sup>1</sup>. Along with the circuit design parameters, one could tune the free-running oscillation frequency. According to the ratio of threshold voltage displacement and therefore the frequency shift influenced by the incoming wave power, one can estimate the bandwidth needed for the variation of  $f_{osc}$ . In this case we have the reference frequency at 3250 Hz with a frequency shift of 350 Hz corresponding to the maximum power we applied (0 dBm). On top of all, the integration time in this case determines the duration

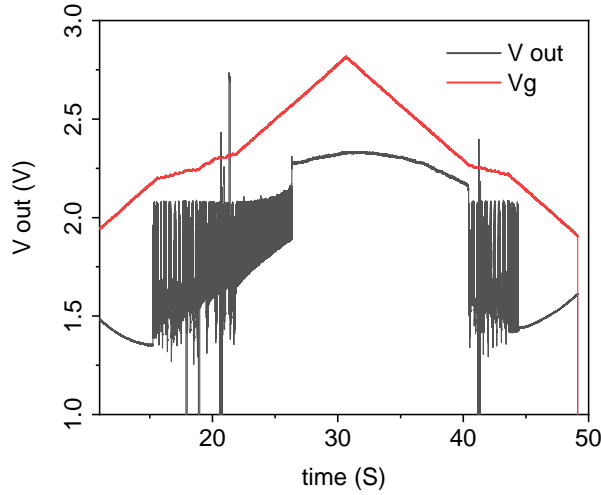


**Figure 6.** Operating region of the spike generator

of each acquisition. If we aim for the minimum NEP, we have to use more cycles of the same measurement, at least about 100 ms according to Allan method for this experiment: fig. 6 (c) of the paper.

The output RF frequency of the VNA is up-converted by mm-wave modules (multipliers) connected as extensions to it. The high-frequency signal is then directed to the CPW through GSG infinity probes. The whole setup for the astable is revealed in fig 7(a). This setup is associated with fig. 1 (c) of the paper. The wafer including VO<sub>2</sub> samples along with the infinity probes are shown in fig. 7(b)

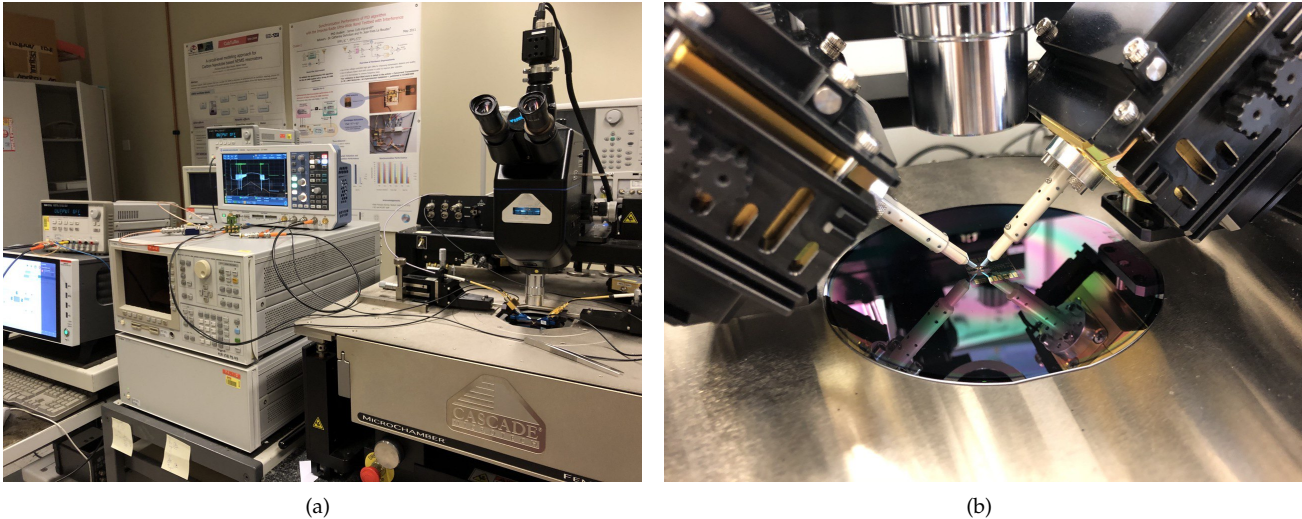


**Figure 7.** (a) Experimental setup for astable circuit, (b) On-wafer VO<sub>2</sub> devices along with the millimeter-wave (mm-wave) GSG infinity probes

#### Supplementary Note 6: Detailed limit of detection (LoD) values

As also indicated in the main text, the minimum detectable signal by the VO<sub>2</sub> two-terminal devices is measured experimentally as 20nW (fig. 6 (b) in the paper). This is while at any power level the additional uncertainty of detection should be considered separately. We calculated the LoD of the detector based on  $3\sigma/R_V$  at different stages as shown in table 1. The LoD degrades by temperature as the responsivity decays by getting closer to the

phase change critical temperature.

Configuration	-30 dBm	-20 dBm	-10 dBm	0 dBm
CPW (RT)	67.8	245.7	758.5	2239.2
CPW (40°C)	124.9	562.4	1703.2	5980.1
CPW (50°C)	2621.6	10068.7	43736.8	185312.
Antennas (RT)	959.2	3736.3	11332.1	33832.3

**Table 1.** The LoD of the detector in different temperatures, based on  $3\sigma/R_V$  of the IMT threshold voltages statistics. All the units in nW.

#### Supplementary Note 7: CPW S parameters

The spectra of the S parameters for the CPW-based devices are shown in figs. 8(a) and 8(b). By the temperature elevation and therefore the  $\text{VO}_2$  interruption becoming more conductive, the spectra become closer to a simple CPW characteristics.

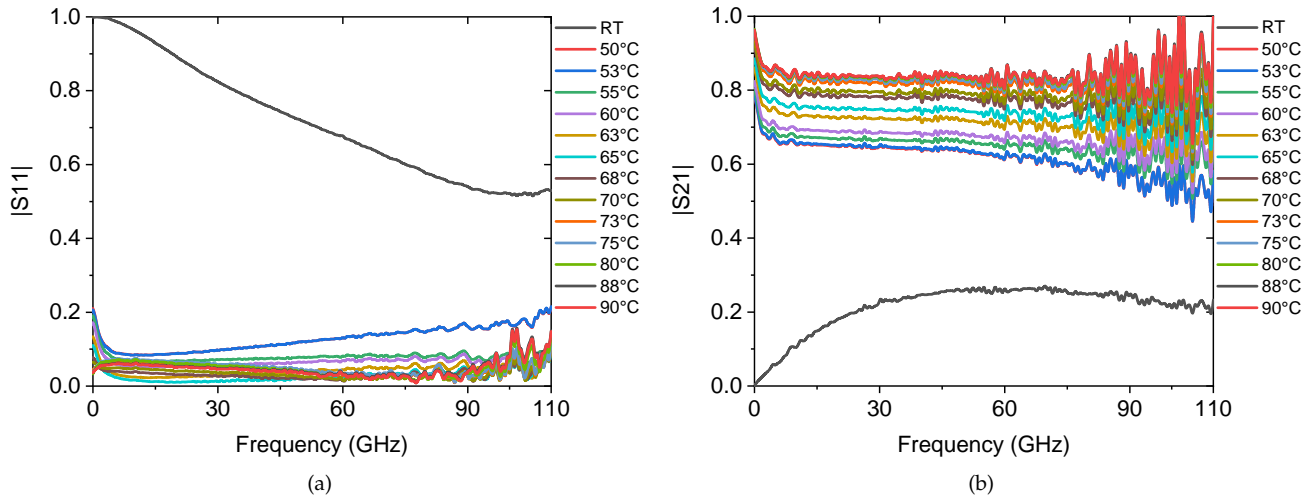


**Figure 8.** S parameters spectra by temperature (a)  $|S_{11}|$ , (b)  $|S_{21}|$

#### References

1. M. Jerry, H. P. D. G. S., N. Shukla & Datta, S. Dynamics of electrically driven sub-nanosecond switching in vanadium dioxide. *IEEE Silicon Nanoelectron. Work. (SNW)* 26–27 (2016).